IEEE Access
Multidisciplinary ⋮ Rapid Review ⋮ Open Access Journal

Received March 31, 2022, accepted April 24, 2022, date of publication May 13, 2022, date of current version May 19, 2022.

Digital Object Identifier 10.1109/ACCESS.2022.3174563

Analysis of Amplitude and Angle of Crosstalk in Frequency Domain of Three-Core Twisted Wires

HONGYAN SUN[1], WENTAO XU[2], WU ZHANG[2], MENGXIA ZHOU[2], AND WEI YAN[2]
[1]College of Taizhou, Nanjing Normal University, Taizhou 225300, China
[2]School of Electrical and Automation Engineering, Nanjing Normal University, Nanjing 210046, China

Corresponding author: Mengxia Zhou (61239@njnu.edu.cn)

ABSTRACT In this paper, a geometric model of multi-core twisted wire is established to analyze the amplitude-frequency and angular-frequency characteristics of crosstalk in electromagnetic compatibility (EMC). The random combination of the cross-section of the multi-core twisted wire is used to accurately simulate the randomness of the actual multi-core twisted wire. The rotation transformation of the cross-section and the random transposition transformation between the conductors and the neural network model are used to obtain the per unit length (p.u.l) parameters at any position. And bring it into the method of chain parameters to find the crosstalk. The results show that the crosstalk amplitude-frequency and angular-frequency characteristics of the different cores of the multi-core twisted wire under the fixed model are very similar. Under the random model, the crosstalk of multi-core twisted wires is very close in the low frequency range, and satisfies a certain envelope value in the high frequency range. Through comparison with full-wave simulation, the reliability of the proposed method is proved.

INDEX TERMS Crosstalk, multi-core twisted wires, neural network algorithm, chain parameter, electromagnetic compatibility (EMC).

I. INTRODUCTION

The multi-core twisted wire used in various electrified systems has the characteristics of small coupling and low noise [1]–[3]. Although it has good performance and characteristics, it is susceptible to external electromagnetic interference in today's complex electromagnetic environment. Among them, crosstalk becomes the main noise in the electromagnetic compatibility (EMC) of multi-core twisted wires [3], [4].

The original multi-core stranded wire model was twisted pair (TWP). Moser and Spencer initially studied the low coupling characteristics of TWP, the magnetic field radiated by the twisted pair, and the radiation sensitivity (RS) [5]. Later, Paul and McKnight proposed the use of transmission line cascade transmission line theory (TLT) to deal with TWP [6]–[8]. After that, the processing and modeling methods of multi-core stranded wires have been proposed successively [9], [10], and the processing methods of crosstalk between wires and multi-core twisted wires [11], [12]. In [13], the crosstalk between multi-core twisted wires with equal torque ratio and unequal torque ratio was compared, and [14] proposed a multi-conductor transmission line for analyzing the crosstalk of shielded random twisted pair bundles.

In addition to studying crosstalk, [15] studied the influence of non-uniform torque on the reliability of twisted wire radiation, and [16] studied the random response of non-uniform multi-strand twisted pair (MTB-TWP) excited by random plane waves. Among various models, [17], [18] proposed a method for predicting the response of multiple TWP beams when a ground plane is irradiated by a plane wave electromagnetic field.

In this paper, an ideal cross-sectional model of uniform twist is established, and based on this, the neural network method and matrix transposition idea are adopted to obtain the cross-sectional model of random twist. The BAS optimization algorithm is used to optimize the neural network model to obtain the global optimal value. Using the chain parameter model, the amplitude-frequency and angular-frequency characteristics of crosstalk are analyzed.

This paper is organized as follows. In Section II, an ideal twisted multi-core stranded wire model is established, and the wire transposition when random twisting occurs is

The associate editor coordinating the review of this manuscript and approving it for publication was Sunil Karamchandani.

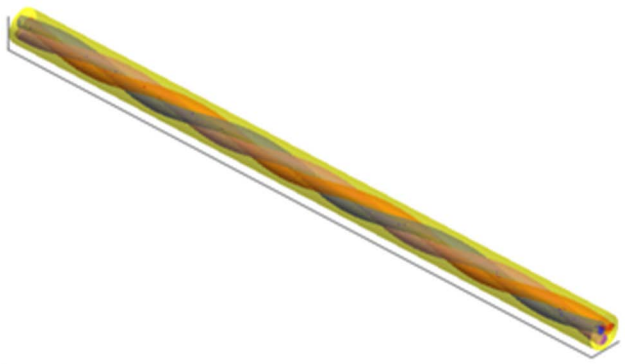

FIGURE 1. Multi-core twisted wire harness model.

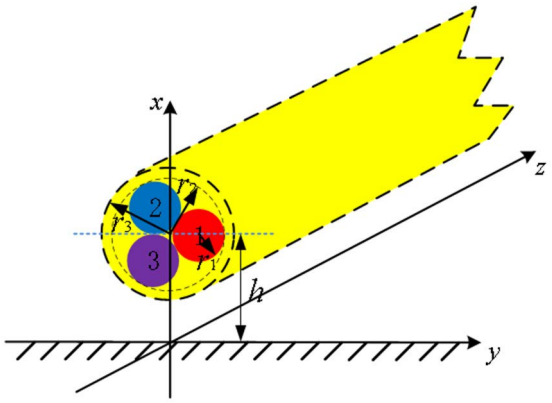

FIGURE 2. Geometry and parameters.

discussed. In Section III, the p.u.l parameters at any position are obtained through the idea of random twisting and matrix transposition. Secondly, combined with the neural network numerical simulation technology of the transmission line matrix (TLM) method is given in Section IV, and the crosstalk amplitude-frequency characteristics and corner-frequency characteristics are analyzed. It is summarized in Section V.

II. MODEL OF MULTI-CORE TWISTED WIRES

A. GEOMETRIC MODEL

In an ideal situation, the multi-core twisted wire harness is evenly twisted inside the core, with a uniform fixed twisting pitch, and the outside is wrapped with a certain thickness of insulating layer, as shown in Fig. 1. However, in common engineering practice, multi-core stranded wires will have random non-uniform twists due to artificial and environmental influences, which are essentially non-uniform transmission lines.

The geometric structure and parameters of a three-core conductor as an example are shown in Fig. 2. The wires are all cylindrical bare wires, the wire radius is r_1, the height of the twisted center is h, the radius from the twisted circumference of the three wires to the twisted center is r_2, and the radius of the outer insulating layer is r_3. The wire

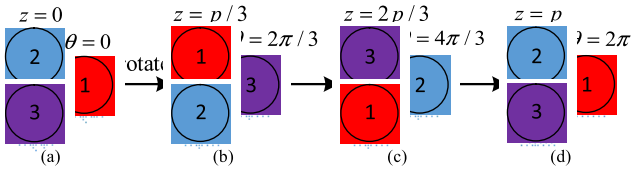

FIGURE 3. Sections and rotation angles corresponding to different z values.

is twisted along the z-axis, and the length of the multi-core stranded wire is L. The position of the center point of the three wires is $\vec{l}_{red}, \vec{l}_{blue}, \vec{l}_{purple}$. Under the same abscissa z, taking $r = r_2 - r_1$, they can be expressed as:

$$\begin{cases} \vec{l}_r(x_1, y_1, z) = r\cos\theta\vec{a}_x + (h + r\sin\theta)\vec{a}_y + z\vec{a}_z \\ \vec{l}_b(x_2, y_2, z) = r\cos(\theta + \frac{2\pi}{3})\vec{a}_x + (h + r\sin(\theta + \frac{2\pi}{3}))\vec{a}_y \\ \qquad\qquad + z\vec{a}_z \\ \vec{l}_p(x_3, y_3, z) = r\cos(\theta + \frac{4\pi}{3})\vec{a}_x + (h + r\sin(\theta + \frac{4\pi}{3}))\vec{a}_y \\ \qquad\qquad + z\vec{a}_z \end{cases} \tag{1}$$

where $\vec{a}_x, \vec{a}_y, \vec{a}_z$ represents the unit vector of the x, y, and z-axes, respectively. θ is the cross-section rotation angle at each position z.

Fig. 3 shows the transposition of the wires corresponding to the twisting of the three-core twisted wire in a pitch. It can be seen that the cross-sectional rotation angle θ and the position z at the initial position of the cross-section show a periodic change.

Taking into account the process of establishing the random three-core twisted wire harness model, the corresponding cross-section and rotation angle under each z value are random, and can be randomly generated by the rotation angle of the ideal three-core stranded wire. Then the rotation angle of the cross-section in each section of three-core twisted wire is:

$$\theta = \begin{cases} \dfrac{2\pi z}{p}, & \text{Ideal model} \\ \text{rand(z)}, & \text{Random model} \end{cases} \tag{2}$$

B. EQUIVALENT CIRCUIT

The large electromagnetic noise interference to the multi-core twisted wire is mainly expressed by the line-to-line crosstalk. Fig. 4 shows the terminal conditions at both ends of the multi-core twisted wire model and the equivalent circuit p.u.l of the multi-core twisted wire.

In [2], the voltage and current of the transmission line satisfy the following equation:

$$\begin{cases} \dfrac{d}{dz}\mathbf{V}(z) = -\mathbf{Z}(z)\mathbf{I}(z) \\ \dfrac{d}{dz}\mathbf{I}(z) = -\mathbf{Y}(z)\mathbf{V}(z) \end{cases} \tag{3}$$

Among them, $\mathbf{V}(z)$ and $\mathbf{I}(z)$ represent the voltage and current vectors at different positions. $\mathbf{Z}(z)$ and $\mathbf{Y}(z)$ represent the corresponding impedance and admittance at different

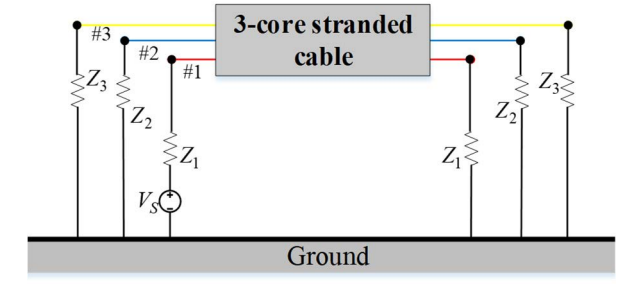

(a) Termination impedance and power supply

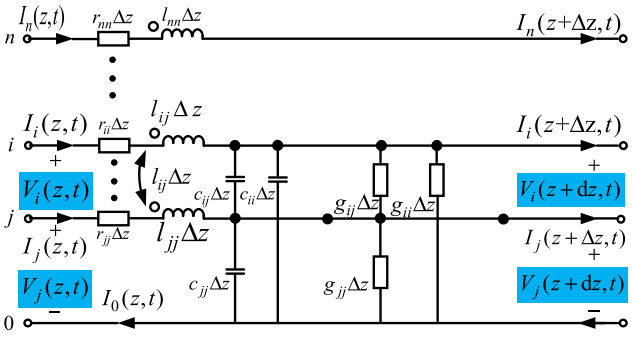

(b) Multi-conductor transmission line unit equivalent circuit.

FIGURE 4. Terminal conditions and equivalent circuit. (a) Termination impedance and power. (b) Multi-conductor transmission line unit equivalent circuit.

positions, which can be expressed as:

$$\begin{cases} \mathbf{Z}(z) = \mathbf{R}(z) + jw\mathbf{L}(z) \\ \mathbf{Y}(z) = \mathbf{G}(z) + jw\mathbf{C}(z) \end{cases} \tag{4}$$

Among them, $\mathbf{R}(z)$, $\mathbf{L}(z)$, $\mathbf{C}(z)$, and $\mathbf{G}(z)$ respectively represent the resistance, inductance, capacitance, and conductance matrices of the corresponding cross-sections at different positions, that is, the p.u.l parameter matrix. They are all symmetric matrices of order n×n. w is the angular frequency of the signal source.

For the convenience of modeling and the unity of description, these four parameter matrices are all represented by $\mathbf{M}$. In the evenly twisted three-core twisted wire model, the rotation of the twisted wire is uniform. Therefore, the parameter matrix $\mathbf{M}$ of the uniform cross-sectional model within $0^o \sim 120^o$, $120^o \sim 240^o$, $240^o \sim 360^o$ is the same. But the location is different, as long as the corresponding transformation is carried out.

$$\mathbf{M}(\theta') = \begin{cases} \mathbf{P}\mathbf{M}(\theta)\mathbf{P}^T, & \theta' \in [120°, 240°) \\ \mathbf{P}^2\mathbf{M}(\theta)(\mathbf{P}^T)^2, & \theta' \in [240°, 360°) \end{cases} \tag{5}$$

where $\theta \in [0°, 120°)$ and $\mathbf{P}$ is the rotation matrix, in the model of this article:

$$\mathbf{P} = \begin{bmatrix} 0 & 0 & 1 \\ 1 & 0 & 0 \\ 0 & 1 & 0 \end{bmatrix} \tag{6}$$

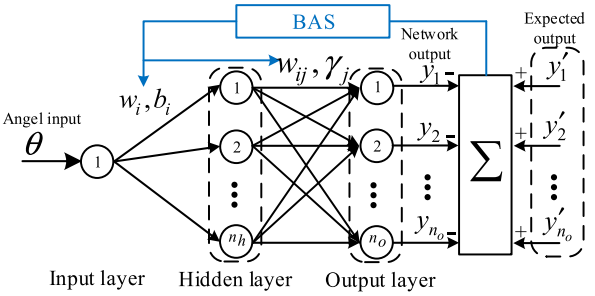

FIGURE 5. BAS-BP neural network topology.

In an ideal conductor, in some cases, if the harness of the transmission line has strong conductivity and good insulation properties, it can be regarded as a lossless ideal conductor, that is, $\mathbf{R}(z)=\mathbf{G}(z)=0$. And the corresponding multi-conductor transmission line equation degenerates to:

$$\begin{cases} \dfrac{d}{dz}\mathbf{V}(z) = -jw\mathbf{L}(z)\mathbf{I}(z) \\ \dfrac{d}{dz}\mathbf{I}(z) = -jw\mathbf{C}(z)\mathbf{V}(z) \end{cases} \tag{7}$$

III. P U L PARAMETERS AND CORSSTALK SOLUTION

A. OBTAINING THE PARAMETERS OF P.U.L

Because the RLCG parameter at different positions are different, but due to the geometric characteristics of the multi-core stranded wire, only the parameters of $0^o \sim 120^o$ are needed to obtain the matrix parameter matrix average at any angle.

However, different positions z correspond to different parameter matrices, and it is difficult to obtain a parameter matrix of any angle in the traditional way. Any certain rotation angle of the cross-section has its unique corresponding parameter matrix, and there is a nonlinear mapping relationship between the rotation angle and the parameter matrix. The transformations of the four parameter matrices are all the same. For simple description, the p.u.l parameter matrix can be expressed as:

$$\mathbf{M}(z) = \begin{bmatrix} m_{11} & m_{12} & m_{13} \\ m_{21} & m_{22} & m_{23} \\ m_{31} & m_{32} & m_{33} \end{bmatrix} \tag{8}$$

where m_{ij} represents the specific resistance value r_{ij}, inductance value l_{ij}, capacitance value c_{ij} and conductance value g_{ij} corresponding to different parameter matrices. And $\mathbf{M}$ is a symmetric matrix, $m_{ij} = m_{ji}$. There is a complex mathematical relationship with the angle, so the neural network optimized by the BAS method can be used to describe this complex mapping relationship. The network topology is shown in Fig. 5.

In the network, the number of input layers is 1, that is, the input is the cross-section rotation angle, the number of hidden layers is n_h, and the number of output layers is n_o. That is, the output is the column vector formed by the upper triangular elements of the parameter matrix in equation (8).

$$Y = [m_{11}, m_{12}, m_{13}, m_{22}, m_{23}, m_{33}]^T \tag{9}$$

The weights and thresholds w_i, b_i and w_{ij}, γ_j are optimized using the BAS optimization algorithm. The specific steps are as follows:

(1) Determine the optimized objective function.

The output value of the network is:

$$y_j = \sum_{i=1}^{n_h} \frac{w_{ij}}{1 + e^{-w_i\theta + b_i}} + \gamma_j \tag{10}$$

Arrange all the weights and thresholds to indicate the position of the long-horned beetle in the high-dimensional space:

$$w = \left[w_1, \cdots, w_i, b_1, \cdots, b_i, w_{11}, \cdots, w_{ij}, \gamma_1, \cdots, \gamma_j\right]^T \tag{11}$$

For N groups of data, the mean square deviation between the network output value and the actual value is:

$$f(w) = E(w_i, w_{ij}) = \frac{1}{2N} \sum_{i=1}^{N} \sum_{j=1}^{n_o} \left(y_j - y_j'\right)^2 \tag{12}$$

Among them, y_j' is the actual given parameter matrix data value, and $f(w)$ is the optimized objective function.

(2) Initialize the position and direction of the long-horned beetle and the optimal value f_{best} of the objective function.

$$w^0 = rands\,(k, 1) \tag{13}$$

Here w represents the initial position of the longhorn beetle in the high-dimensional data space. k represents the dimension of the weight vector, and *rands* represents the generation of a row vector that obeys a uniform distribution.

The direction of longhorn is:

$$S^{\rightarrow} = \frac{rands\,(k, 1)}{\|rands\,(k, 1)\|_2} \tag{14}$$

In the formula, $\|rands(k, 1)\|_2$is the 2-norm of the column vector.

(3) Establish the position vector of the beetle's left beard and the beetle's right beard

$$w_r^t = w^t + d^t \bullet \vec{S}/2 \tag{15}$$

$$w_r^t = w^t - d^t \bullet \vec{S}/2 \tag{16}$$

In the formula, t is the number of iterations, and the horizontal distance between the two whiskers is d.

(4) Let f be the function to be optimized for the algorithm, that is, the odor intensity of longhorn beetle search. For BP neural network problems, it is generally the mean square error. According to the position of the left and right whiskers and the odor intensity of the beetle at the current moment, the search direction of the beetle is judged: if $f\left(w_l^t\right)$ is less than $f\left(w_r^t\right)$, the beetle searches to the left; otherwise, it searches to the right.

$$w^{t+1} = w^t + \delta^t \bullet \vec{S} \bullet sign\left(f\left(w_r^t\right) - f\left(w_l^t\right)\right) \tag{17}$$

In the formula, δ^t represents the step size factor under t iterations, *sign* is a sign function, and the output result is plus or minus 1.

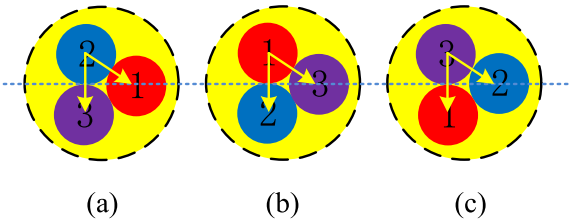

FIGURE 6. The situation where random transposition occurs.

(5) Iteratively update the beetle step length and the distance between the beetle's left and right whiskers.

$$d^{t+1} = 0.95d^t + 0.01 \tag{18}$$

$$\delta^{t+1} = 0.95\delta^t \tag{19}$$

Generally, the initial step size is $\delta = \sqrt{k}$. For the new w^{t+1}, the position of the longhorn beetle in the search direction can be obtained, and the next iteration calculation can be performed. Until the maximum number of iterations is reached or the minimum error value is met, the iteration is stopped, so as to obtain the global minimum of the average error.

1.3Taking the cross-section of the wire harness with a rotation degree of 0° in Fig. 3(a). as the reference cross-section, the corresponding three-core twisted wire model is established in the Ansys Q3D simulation software. It can be seen from Fig. 3 that the RLCG parameter matrix of the entire pitch can be obtained only by extracting the RLCG parameter matrix of the twisted wire within 1/3 of the pitch. Starting from 0°, extract a sample of the R, L, C, G parameter matrix for the three-core twisted wire at equal intervals of 3°, and end at 117°, forty sets of training samples can be obtained.

B. P.U.L PARAMETERS OF THE RANDOM MODEL

After the network is trained with pre-extracted data, it can predict the p.u.l parameter matrix at any rotation angle. Taking into account the symmetry of the cross-section of the multi-core twisted wire harness and the periodicity of the rotation angle, the angle of the training network only needs to be 0º ∼120º.

When considering the situation of non-uniform twisting, random transpositions between the wires will occur, as shown in Fig. 6.

When two or more wires are randomly transposed in the wiring harness, the corresponding parameter matrix $\mathbf{M}'$ after the position exchange can use the transformation matrix $\mathbf{T}$ to represent the conversion of the unit length parameter matrix before and after the transposition, which is expressed as:

$$\mathbf{M}' = \mathbf{T}_{ij}^{(k)} \cdots \mathbf{T}_{ij}^{(1)} \mathbf{M} \mathbf{T}_{ij}^{(1)} \cdots \mathbf{T}_{ij}^{(k)} \tag{20}$$

where k is the number of transpositions, and $1 \leq k \leq n-1$, n is the number of cores. T is the transformation matrix when transposition occurs between the i-th conductor and the j-th

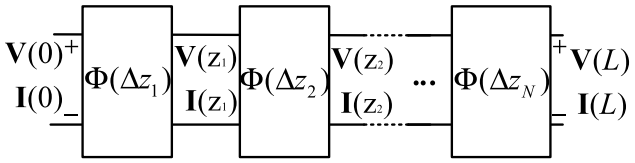

FIGURE 7. Transmission line chain parameter model.

conductor, expressed as:

$$\mathbf{T}_{ij}^{(k)} = \begin{bmatrix} 1 & 0 & \cdots & 0 & \cdots & 0 & \cdots & 0 \\ 0 & 1 & \cdots & 0 & \cdots & 0 & \cdots & 0 \\ \vdots & \vdots & \ddots & \vdots & \vdots & \vdots & \vdots & \vdots \\ 0 & 0 & \cdots & 0 & \cdots & 1(i) & \cdots & 0 \\ \vdots & \vdots & \vdots & \vdots & \ddots & \vdots & \vdots & \vdots \\ 0 & 0 & \cdots & 1(j) & \cdots & 0 & \cdots & 0 \\ \vdots & \vdots & \vdots & \vdots & \vdots & \vdots & \ddots & \vdots \\ 0 & 0 & \cdots & 0 & \cdots & 0 & \cdots & 1 \end{bmatrix} \tag{21}$$

C. SOLVE CROSSTALK BY CHAIN PARAMETERS

Through the discussion in the previous section, different positions z and cross-section rotation angles can be transformed into each other. In the uniformly twisted multi-core stranded wire model, the p.u.l within 0^o $\sim 120^o$ can be obtained through BAS-BPNN. The p.u.l within $120^o \sim 240^o$, $240^o \sim 360^o$ can be obtained by transformation of the rotation matrix $\mathbf{P}$. In the multi-core stranded wire of the random model, the p.u.l within 0^o $\sim 120^o$ can still be obtained by BAS-BPNN, but the p.u.l generated by the random transposition of its conductor can be obtained by the transposition matrix $T_{ij}^{(k)}$ transformation.

Considering the terminal impedance and power supply in Fig. 4, the transmission line equation can be converted to analog [3].

$$\begin{cases} \mathbf{V}(z) = \mathbf{T}_V(z)\,\mathbf{V}_m(z) \\ \mathbf{I}(z) = \mathbf{T}_I(z)\,\mathbf{I}_m(z) \end{cases} \tag{22}$$

The original equation can be reduced to:

$$\begin{cases} \dfrac{d^2}{dz^2}\mathbf{V}_m(z) = \mathbf{T}_V^{-1}(z)\,\mathbf{Z}(z)\,\mathbf{Y}(z)\,\mathbf{T}_V(z)\,\mathbf{V}_m(z) = r^2\mathbf{V}_m(z) \\ \dfrac{d^2}{dz^2}\mathbf{I}_m(z) = \mathbf{T}_I^{-1}(z)\,\mathbf{Y}(z)\,\mathbf{Z}(z)\,\mathbf{T}_I(z)\,\mathbf{I}_m(z) = r^2\mathbf{I}_m(z) \end{cases} \tag{23}$$

where r^2 is a diagonal matrix of $n \times n$, and $T_V^T = T_I^{-1}$.

Reconsider formula (4) and use ports to characterize the relationship between voltage and current. As shown in Fig. 7, it is a chain parameter port based on the cascade concept.

Therefore, the voltage and current of each port satisfy:

$$\begin{bmatrix} \mathbf{V}(\Delta z_k) \\ \mathbf{I}(\Delta z_k) \end{bmatrix} = \mathbf{\Phi}(\Delta z_k) \begin{bmatrix} \mathbf{V}(\Delta z_{k-1}) \\ \mathbf{I}(\Delta z_{k-1}) \end{bmatrix} \tag{24}$$

As shown in Fig. 7, get different chain parameter matrix:

$$\mathbf{\Phi}(\Delta z_k) = \begin{bmatrix} \phi_{11}(\Delta z_k) & \phi_{12}(\Delta z_k) \\ \phi_{21}(\Delta z_k) & \phi_{22}(\Delta z_k) \end{bmatrix} \tag{25}$$

where $\phi_{11}(\Delta z_k)$, $\phi_{12}(\Delta z_k)$, $\phi_{21}(\Delta z_k)$, $\phi_{22}(\Delta z_k)$ are the chain parameter subarrays, they are:

$$\begin{cases} \phi_{11}(\Delta z_k) = \dfrac{1}{2}\mathbf{Y}^{-1}\mathbf{T}_I\left(e^{r\Delta z_k} + e^{-r\Delta z_k}\right)\mathbf{T}_I^{-1}\mathbf{Y} \\ \phi_{12}(\Delta z_k) = -\dfrac{1}{2}\mathbf{Y}^{-1}\mathbf{T}_I\left(e^{r\Delta z} - e^{-r\Delta z_k}\right)\mathbf{T}_I^{-1} \\ \phi_{21}(\Delta z_k) = -\dfrac{1}{2}\mathbf{T}_I\left(e^{r\Delta z_k} - e^{-r\Delta z_k}\right)r^{-1}\mathbf{T}_I^{-1}\mathbf{Y} \\ \phi_{22}(\Delta z_k) = \dfrac{1}{2}\mathbf{T}_I\left(e^{r\Delta z_k} + e^{-r\Delta z_k}\right)\mathbf{T}_I^{-1} \end{cases} \tag{26}$$

Combining the BSAS-BPNN algorithm to obtain the p.u.l at any position z, all the chain parameters $\mathbf{\Phi}(z)$ can be obtained by using formula (26).

The chain parameters of the transmission line are:

$$\mathbf{\Phi}(L) = \prod_{k=1}^{N} \mathbf{\Phi}_{N-k+1}(\Delta z_{N-k+1}) \tag{27}$$

where N is the divided length of the transmission line, the voltage and current between the near end (z=0) and the far end (z= L) of the transmission line satisfy:

$$\begin{bmatrix} \mathbf{V}(L) \\ \mathbf{I}(L) \end{bmatrix} = \mathbf{\Phi}(L) \begin{bmatrix} \mathbf{V}(0) \\ \mathbf{I}(0) \end{bmatrix} \tag{28}$$

The terminal constraints are:

$$\begin{cases} \mathbf{V}(0) = \mathbf{V}_S - \mathbf{Z}_S\mathbf{I}(0) \\ \mathbf{V}(L) = \mathbf{V}_L + \mathbf{Z}_L\mathbf{I}(L) \end{cases} \tag{29}$$

where $\mathbf{V}_S = [V_S;0;0]^T$ is the near-end termination voltage source, and $\mathbf{Z}_S$ is the near-end termination impedance. $\mathbf{V}_L = [0;0;0]^T$ is the far-end termination voltage source, and $\mathbf{Z}_L$ is the far-end termination impedance.

Find the near-end crosstalk (NEXT) and far-end crosstalk (FEXT) as:

$$\begin{cases} \text{NEXT} = 20\log_{10}(|\mathbf{V}(0)|/V_s) \\ \text{FEXT} = 20\log_{10}(|\mathbf{V}(L)|/V_s) \end{cases} \tag{30}$$

IV. NUMERICAL EXPERIMENT VERIFICATION AND ANALYSIS

The wire used in this paper is a copper core wire, the wire radius r_1 =0.335mm, the radius of the ring enclosed by the three wires is r_2 =0.722mm, the outermost insulating material is PVC, and the radius from the center of the circle is r_3 =1.022mm. The length of the transmission line is L = 1m, and the height above the ground is h = 15mm. The transmission line is divided into N = 2000 sections in total.

Through the finite element method (FEM), a small amount of pul parameter matrix is obtained at 0^o $\sim 120^o$ for network training. The unit of p.u.l parameter matrix $\mathbf{R}$(z), $\mathbf{L}$(z), $\mathbf{C}$(z), $\mathbf{G}$(z) is Ω/m, nH/m, pF/m, mS/m.

Fig. 8 shows the simulation in CST. The model is an ideal model with uniform twisting for 20 cycles. The near-end and far-end crosstalk of the transmission line are solved by the TLM method and compared with the method proposed in this article.

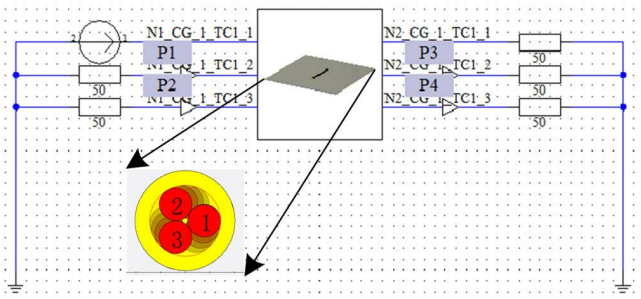

FIGURE 8. Simulation model in CST.

TABLE 1. Average and maximum error of amplitude in next (dB).

Wire	0.1MHz-0.1GHz	0.1GHz-0.5GHz	0.5GHz-1GHz	MIN	MAX
2	0.3009	0.3081	0.3947	0.0069	2.0622
3	0.3004	0.3051	0.3927	0.0067	2.1480

TABLE 2. Average and maximum error of amplitude in fext (dB).

Wire	0.1MHz-0.1GHz	0.1GHz-0.5GHz	0.5GHz-1GHz	MIN	MAX
2	1.1378	1.6892	1.7709	0.0013	3.6371
3	1.1942	1.7692	1.8506	0.0011	3.8153

A. THE AMPLITUDE-FREQUENCY CHARACTERISTICS OF CROSSTALK IN THE IDEAL MODEL

In the ideal multi-core stranded wire model, the method in this paper is used to apply a voltage source on the conductor 1, and the frequency range of the power supply is from 0.1MHz to 1GHz. The comparison of the results of calculating the amplitude-frequency characteristics of the crosstalk of No. 2 and No. 3 wire with the results based on the TLM method are shown in Fig. 9 and 10, respectively. It can be seen that it has a higher degree of agreement, the effect in the middle frequency band is better than the effect in the low frequency band ($f < 100$MHz) and the high frequency band ($f > 500$MHz), and the trend of change is very similar to the peaks and valleys. This can prove the reliability of the method in this paper.

It can be seen that the NEXT and FEXT amplitude-frequency characteristic curves of No. 2 wire and No. 3 wire are very close. This is because the power is applied to No. 1 conductor and the disturbed No. 2 and No. 3 wire are symmetrically distributed with each other. In addition, the results of FEXT in the two conductors and CST vary greatly in the mid-frequency range, while NEXT varies less in the high-frequency range. This may be because NEXT is closer to the power supply and is more affected. The maximum value of NEXT is close to about −10dB, and the maximum value of FEXT is close to about −14dB.

Table 1 and Table 2 respectively show the average error and maximum value of the amplitude of NEXT and FEXT in different frequency ranges. It can be seen that the minimum error of NEXT is greater than FEXT, while the maximum

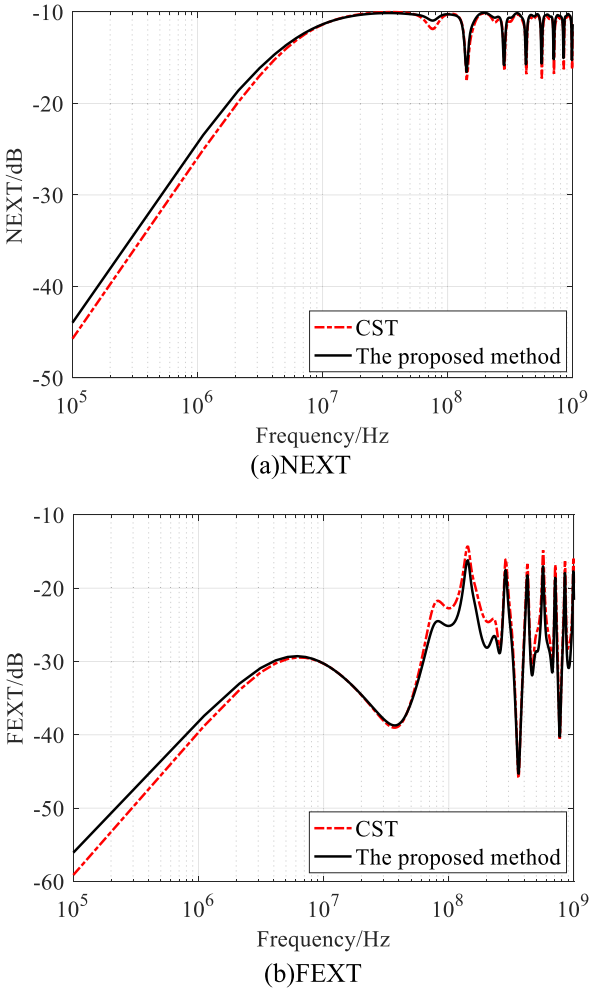

FIGURE 9. Amplitude-frequency characteristics of crosstalk in No. 2 wire. (a) NEXT. (b) FEXT.

error is less than FEXT, and the maximum error of No. 3 wire is greater than that of No. 2 wire. The maximum error of NEXT is 2.1480dB, and the maximum error of FEXT is 3.8153dB.

From the perspective of different frequency ranges, the average error of NEXT of No. 2 wire is less than that of No. 3 wire, and the average error of FEXT of No. 2 wire is greater than that of No. 3 wire. In the range of 0.5GHz-1GHz, the average error of NEXT and FEXT both reach the maximum.

B. THE ANGULAR-FREQUENCY CHARACTERISTICS OF CROSSTALK IN THE IDEAL MODEL

Similarly, the comparison of the angular frequency characteristics of the crosstalk of No. 2 and No. 3 wire with the results based on the TLM method are shown in Fig. 11 and 12, respectively. It can be seen that there is a similar agreement with the amplitude-frequency characteristics.

The difference is that the results of the corner frequency characteristics in the low frequency band ($f < 100$MHz) are

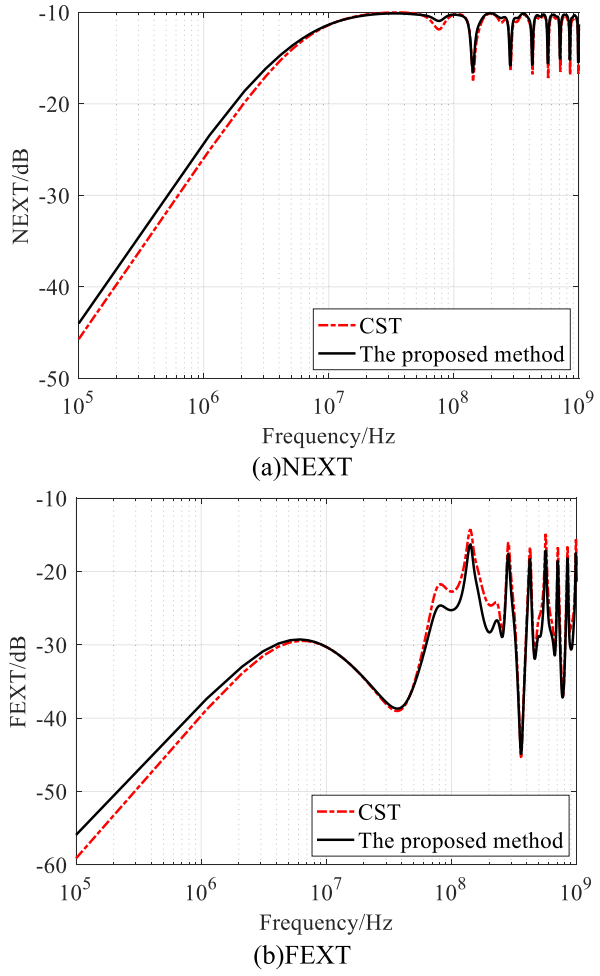

FIGURE 10. Amplitude-frequency characteristics of crosstalk in No. 3 wire. (a) NEXT. (b) FEXT.

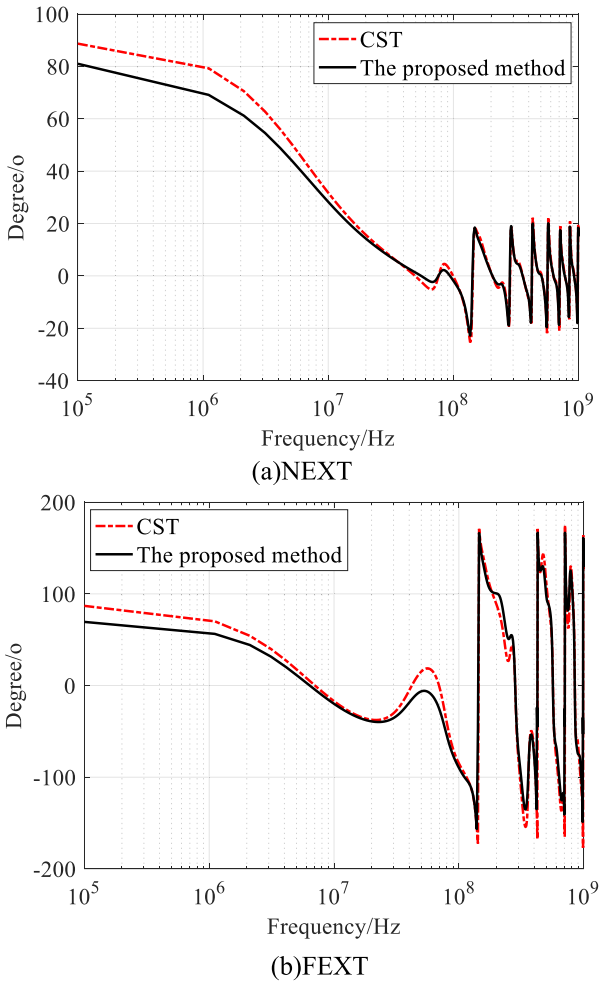

FIGURE 11. Angular-frequency characteristics of crosstalk in No. 2 wire. (a) NEXT. (b) FEXT.

TABLE 3. Average and maximum error of the angular in next (o).

Wire	0.1MHz-0.1GHz	0.1GHz-0.5GHz	0.5GHz-1GHz	MIN	MAX
2	2.1495	1.1015	1.5210	0.0091	13.3689
3	1.9883	1.0145	1.2984	0.0014	12.4132

TABLE 4. Average and maximum error of the angular in fext (o).

Wire	0.1MHz-0.1GHz	0.1GHz-0.5GHz	0.5GHz-1GHz	MIN	MAX
2	12.5001	12.2882	11.0842	0.0010	27.0645
3	10.0348	11.3769	10.7349	0.1214	24.7086

quite different from the CST results, and the effect is better in the high frequency band ($f > 500$MHz). According to the theory of multi-conductor transmission lines, the parameters R, L, C, and G are related to frequency. In this paper, the influence of frequency on the parameter matrix is ignored [9], and the parameters extracted at 1GHz are used, so the calculation results in the high frequency band close to 1GHz are closer to the actual value. And NEXT has a small change in the high frequency range, and the maximum angle is kept at about $\pm 20°$. The FEXT has a large range of changes in the high frequency range, and the maximum angle remains at about $\pm 180°$.

Table 3 and Table 4 respectively show the average error and maximum value of NEXT and FEXT angles in different frequency ranges. It can be seen that the maximum error of NEXT is also less than FEXT, and the maximum error of No. 3 wire is less than that of No. 2 wire. The maximum error of NEXT is 13.3689°, and the maximum error of FEXT is 27.0645°.

From the perspective of different frequency ranges, the average error of NEXT and FEXT of No. 3 wire is smaller than that of No. 2 wire. In the range of 0.1MHz-0.1GHz, the average errors of NEXT and FEXT reach the maximum of 2.1495° and 12.5001°, respectively.

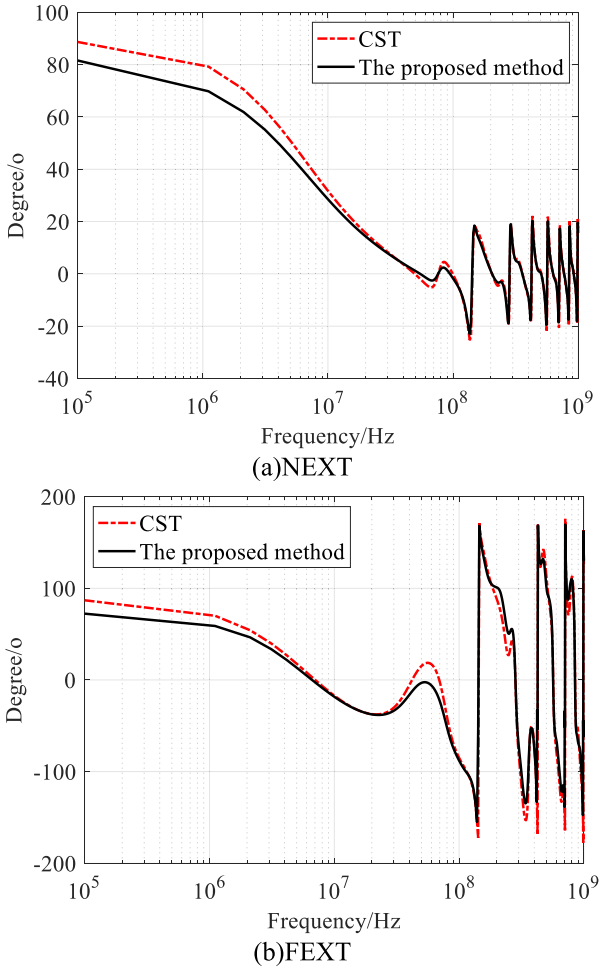

FIGURE 12. Angular-frequency characteristics of crosstalk in No. 3 wire. (a) NEXT. (b) FEXT.

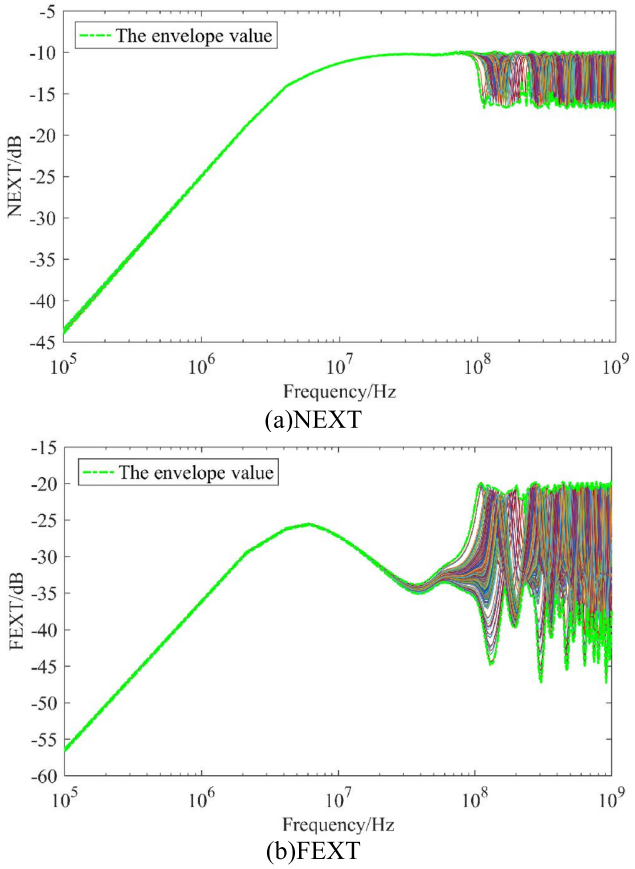

FIGURE 13. Amplitude-frequency characteristics of crosstalk in random model. (a) NEXT. (b) FEXT.

C. THE AMPLITUDE-FREQUENCY AND ANGULAR-FREQUENCY CHARACTERISTICS OF CROSSTALK IN RANDOM MODELS

The amplitude-frequency and angular-frequency characteristics of the random model are shown in Fig. 13 and 14, respectively. Fig. 13(a), 14(a) and Fig. 13(b), 14(b) are NEXT and FEXT, respectively. It calculates a total of 600 models, and there are 1200 corresponding NEXT and FEXT curves each, which more accurately describes the crosstalk characteristics of the random twisted wire model. The green dashed line represents the upper envelope and lower envelope of the crosstalk amplitude-frequency and angular-frequency characteristic. The curves of other colors are the crosstalk characteristic waveforms under different twisting conditions.

It can be seen that both NEXT and FEXT are very close in the low frequency, while the NEXT fluctuation is small in the high frequency, and the FEXT fluctuation is large. And the change of the upper and lower envelopes of NEXT is relatively stable, and the change of the upper and lower envelopes of FEXT is more rapid.

In the high frequency range, the upper envelope value of the amplitude-frequency characteristic curve of NEXT is basically about −10dB, and the lower envelope value is about −17dB. The upper envelope value of the NEXT angular frequency characteristic curve in the high frequency range is basically about 20°, and the lower envelope value is basically about −20°. The FEXT amplitude-frequency characteristic curve has a maximum upper envelope value of about −20dB in the high frequency range, and a large change in the lower envelope value, with a minimum of about −47dB. The FEXT angular frequency characteristic curve changes between ±180°in the high frequency range.

It can be seen that the FEXT amplitude-frequency characteristics and angular frequency characteristics of the three-core stranded wire under different twisting conditions are susceptible to the influence of high-frequency signals, but the influence on NEXT is limited. This may be that FEXT is affected by the accumulation of twisting effects of three-core twisted wires, while NEXT is less affected by changes in twisting conditions. And as the complexity of twisting increases, the curves of NEXT and FEXT will gradually become similar.

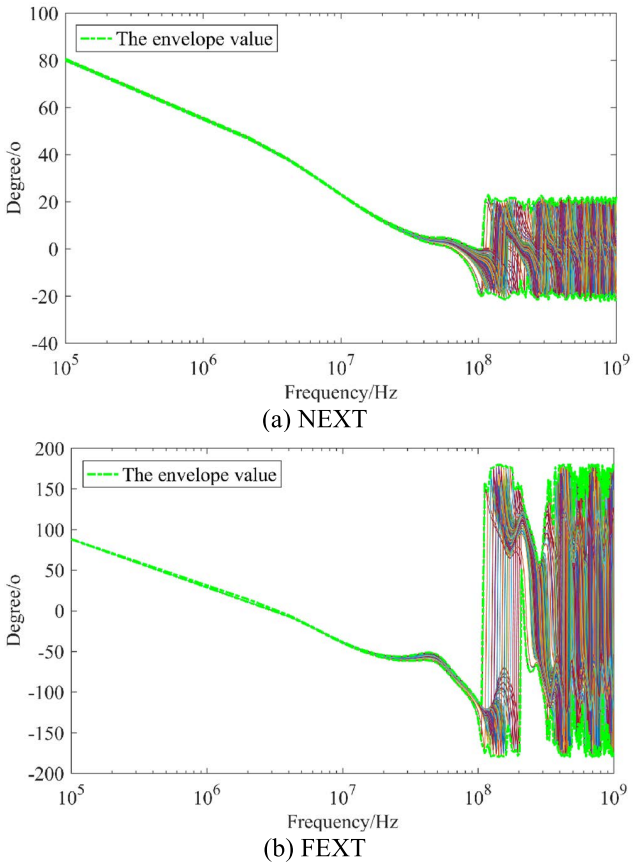

FIGURE 14. Angular -frequency characteristics of crosstalk in random model. (a) NEXT. (b) FEXT.

V. CONCLUSION

In this article, a model of multi-core stranded wire is proposed. The model includes ideal twisting and random twisting, which overcomes the randomness problem in the multi-core twisted wire model in the literature.

In addition, the p.u.l parameter matrix within the rotation angle of part of the cross-section is obtained through the neural network algorithm. Through cross-section rotation matrix transformation and conductor random transposition matrix transformation, the p.u.l parameter matrix at any position is extracted. The crosstalk is solved by the chain parameter method with cascade thought and the amplitude-frequency characteristics and angular-frequency characteristics of NEXT and FEXT are analyzed. And compared with CST simulation based on TLM, it proves that the method in this paper has high reliability.

In the crosstalk characteristic curve, the FEXT characteristic is easily affected by high-frequency signals, and both NEXT and FEXT are less affected in the low frequency range. In different twisting models, the characteristic curves of NEXT and FEXT are kept in a certain envelope range in the high frequency range, especially the envelope value of NEXT presents an approximate horizontal straight line change trend. These influencing factors and results will have important reference significance in subsequent research and engineering applications.

REFERENCES

[1] S. Shiran, B. Reiser, and H. Cory, "A probabilistic method for the evaluation of coupling between transmission lines," *IEEE Trans. Electromagn. Compat.*, vol. 35, no. 3, pp. 387–393, Aug. 1993.

[2] G. Spadacini, F. Grassi, F. Marliani, and S. A. Pignari, "Transmission-line model for field-to-wire coupling in bundles of twisted-wire pairs above ground," *IEEE Trans. Electromagn. Compat.*, vol. 56, no. 6, pp. 1682–1690, Dec. 2014.

[3] A. Shoory, M. Rubinstein, A. Rubinstein, C. Romero, N. Mora, and F. Rachidi, "Application of the cascaded transmission line theory of Paul and McKnight to the evaluation of NEXT and FEXT in twisted wire pair bundles," *IEEE Trans. Electromagn. Compat.*, vol. 55, no. 4, pp. 648–656, Aug. 2013.

[4] F. Grassi and S. A. Pignari, "Immunity to conducted noise of data transmission along DC power lines involving twisted-wire pairs above ground," *IEEE Trans. Electromagn. Compat.*, vol. 55, no. 1, pp. 195–207, Feb. 2013.

[5] C. Taylor and J. Castillo, "On the response of a terminated twisted-wire cable excited by a plane-wave electromagnetic field," *IEEE Trans. Electromagn. Compat.*, vol. EMC-22, no. 1, pp. 16–19, Feb. 1980.

[6] J. R. Moser and R. F. Spencer, "Predicting the magnetic fields from a twisted-pair cable," *IEEE Trans. Electromagn. Compat.*, vol. EMC-10, no. 3, pp. 324–329, Sep. 1968.

[7] C. R. Paul and J. W. McKnight, "Prediction of crosstalk involving twisted pairs of wires—Part I: A transmission-line model for twisted-wire pairs," *IEEE Trans. Electromagn. Compat.*, vol. EMC-21, no. 2, pp. 92–105, May 1979.

[8] R. Paul and J. W. McKnight, "Prediction of crosstalk involving twisted pairs of wires—Part II: A simplified low-frequency prediction model," *IEEE Trans. Electromagn. Compat.*, vol. ECM-21, no. 2, pp. 105–114, May 1979.

[9] C. R. Paul, *Analysis of Multiconductor Transmission Lines*. New York, NY, USA: Wiley, 1994.

[10] X. Liu, F. Grassi, G. Spadacini, and S. A. Pignari, "Physically based modeling of hand-assembled wire bundles for accurate EMC prediction," *IEEE Trans. Electromagn. Compat.*, vol. 62, no. 3, pp. 914–922, Jun. 2020.

[11] S. Sun, G. Liu, J. L. Drewniak, and D. J. Pommerenke, "Hand-assembled cable bundle modeling for crosstalk and common-mode radiation prediction," *IEEE Trans. Electromagn. Compat.*, vol. 49, no. 3, pp. 708–718, Aug. 2007.

[12] S. A. Pignari and G. Spadacini, "Plane-wave coupling to a twisted-wire pair above ground," *IEEE Trans. Electromagn. Compat.*, vol. 53, no. 2, pp. 508–523, May 2011.

[13] G. Spadacini and S. A. Pignari, "Radiated susceptibility of a twisted-wire pair illuminated by a random plane-wave spectrum," *IEICE Trans. Commun.*, vol. 93, no. 7, pp. 1781–1787, 2010.

[14] J. H. G. J. L. Rotgerink and J. Verpoorte, "Low-frequency closed-form expressions for crosstalk between twisted wire pairs," in *Proc. ESA Workshop Aerosp. EMC (Aerospace EMC)*, Valencia, Spain, May 2016, pp. 1–6.

[15] X. Song, J. Wang, B. Li, and D. Su, "Crosstalk model for shielded bundles of random twisted-wire pairs," in *Proc. Asia–Pacific Int. Symp. Electromagn. Compat. (APEMC)*, Shenzhen, China, May 2016, pp. 766–769.

[16] A. Tatematsu, F. Rachidi, and M. Rubinstein, "A technique for calculating voltages induced on twisted-wire pairs using the FDTD method," *IEEE Trans. Electromagn. Compat.*, vol. 59, no. 1, pp. 301–304, Feb. 2017.

[17] O. Gassab, S. Bouguerra, L. Zhou, Z.-G. Zhao, and W.-Y. Yin, "Stochastic analysis of multitwisted cables with random parameters excited by random plane-wave fields," *IEEE Trans. Electromagn. Compat.*, vol. 62, no. 5, pp. 2084–2095, Oct. 2020.

[18] Y. Yan, L. Meng, X. Liu, T. Jiang, J. Chen, and G. Zhang, "An FDTD method for the transient terminal response of twisted-wire pairs illuminated by an external electromagnetic field," *IEEE Trans. Electromagn. Compat.*, vol. 60, no. 2, pp. 435–443, Apr. 2018.

[19] S. Chabane, P. Besnier, and M. Klingler, "A modified enhanced transmission line theory applied to multiconductor transmission lines," *IEEE Trans. Electromagn. Compat.*, vol. 59, no. 2, pp. 518–528, Apr. 2017.

HONGYAN SUN is currently pursuing the degree in control theory and control engineering with the Zhongyuan University of Technology. She is currently an Associate Professor with the College of Taizhou, Nanjing Normal University. Her main research interests include intelligent control and electromagnetic compatibility.

WENTAO XU was born in Jiangsu, China. He received the B.S. degree from the School of Electrical Engineering and Automation, Northeast Electric Power University, Jilin, China, in 2020. He is currently pursuing the master's degree in electrical engineering with Nanjing Normal University, Nanjing, China. His main research interests include multi-conductor transmission lines and EMC.

WU ZHANG was born in Anhui, China. He received the B.S. degree from the School of Electrical Engineering and Automation, Xi'an University of Technology, Xi'an, China, in 2020. He is currently pursuing the master's degree in electrical engineering with Nanjing Normal University, Nanjing, China. His main research interests include multi-conductor transmission lines and EMC.

MENGXIA ZHOU received the M.S. degree in electrical engineering and the Ph.D. degree in physics and electronics from Nanjing Normal University, in 2018 and 2021, respectively. His main research interests include electromagnetic compatibility, electromagnetic environment effect, and high frequency device modeling.

WEI YAN received the M.S. degree in electrical engineering and the Ph.D. degree in physics and electronics from Nanjing Normal University, in 2011 and 2014, respectively. He is currently an Associate Professor with Nanjing Normal University. He is a Senior Member of the China Electrical Technology Association and the Evaluation Expert of the Electromagnetic Compatibility Calibration Specification of China.